

Observation of many-body dressed molecules

fermi1¹, Arthur Christianen, Richard Schmidt

¹MIT-Harvard Center for Ultracold Atoms,
Research Laboratory of Electronics,
and Department of Physics,
Massachusetts Institute of Technology,
Cambridge, Massachusetts 02139, USA

(Dated: June 28, 2023)

The way the properties of particles change in presence of a background field is an essential topic in various fields of physics. Here we demonstrate that this can also be true in case of chemistry. To this end, we prepare a system of fermionic ^{40}K impurities immersed in a Bose-Einstein condensate of ^{23}Na . For weak interactions the Bose polaron quasiparticles which form, are well understood. However, at strong coupling the rules of chemistry enter the game, and the impurity and the bosons can form bound states. We observe the formation of coherent superpositions of dimer and trimer states, which are coupled due to the background condensate. This shows the remarkable role a quantum medium can play in the formation of ultracold molecules.

INTRO

In the standard model of physics, many important properties of the elementary particles are defined by their interaction with background fields, e.g., the Higgs field, which gives all particles their mass, or the electromagnetic field, which mediates the forces between charged particles. Cold atom experiments have proven to be clean realizations of tunable model systems, providing insight into this paradigm from a unique perspective. Indeed, one of the foundations of the field was the production and observation of Bose-Einstein condensates (BEC), demonstrating that composite particles too can serve as a background field and be well-described by field theory. As in the standard model, the BEC as a medium can strongly affect the properties of the particles immersed in it. As a concrete example, we consider the case of a fermionic ^{40}K atom in a BEC of ^{23}Na . The quasiparticle which is formed by this “quantum impurity” dressed by the BEC is called the Bose polaron, after the paradigmatic polaron well known in condensed matter.

At weak coupling the Bose polaron is relatively simple to understand: mean-field theory gives a good description and the quasiparticle properties can be expressed in terms of a set of simple universal variables. However, at strong coupling it becomes apparent that in fact the rules of chemistry describe the interactions between the impurity atom and the atoms from the BEC. The formation of bound states is crucial in this model, marking a clear difference from typical polarons in condensed matter physics.

In the strong coupling regime, the Bose polaron problem is theoretically challenging due to the presence of many-body bound states and correlations. These kinds of states are usually avoided for a fermionic bath, since Pauli blocking prevents more than one fermionic bath particle from binding to the impurity. In the bosonic

case, only the interboson repulsion prevents infinitely many non-interacting bosons from binding or collapsing onto the impurity. Simultaneously, a mobile impurity can mediate attractive interactions, which instead stimulates binding to the impurity. These mediated interactions for example gives rise to the Efimov effect, the existence of a set of universal trimer states despite interactions being too weak to form a dimer. Our study explores this problem by producing such many-body bound states spectroscopically, and our observations provide an excellent testing ground for modern theory.

We see that the background BEC stimulates the formation of a conceptually new quasiparticle, i.e., a coherent superposition of the dimer, trimer, and free impurity states. This is illustrated in Fig. 1. In Fig. 1a) we qualitatively show the mixture we prepare, with the BEC in orange, the bosonic excitations in red and the impurities in blue. In Fig. 1b) we see an effective emerging three-level Hamiltonian, where the “bare” levels correspond to a free impurity, a dimer and a trimer state, and where the off-diagonal coupling between these levels is caused by the BEC. The eigenvalues of this Hamiltonian and the character of the eigenstates in terms of the different free components is shown in Fig. 1c).

The formation of these superposition state appears since the coupling between the dimer and trimer by the BEC is an order of magnitude larger than their difference in binding energies, in contrast to typical molecular spectroscopy. This provides evidence that the eigenstates we observe are strongly mixed, and amplifies the effect of the higher-order correlations in the system, which would otherwise be extremely challenging to observe. This three level mixing matrix is on the one hand similar to the famous Cabibbo–Kobayashi–Maskawa (CKM) matrix describing the mixing of the quarks in the standard model due to the weak force. On the other hand, our results show how fundamental concepts of physics can have a

remarkable effect on chemical processes in a degenerate medium in the form of molecule formation. These insights can potentially have a strong impact on the way how molecules are created at such cold temperatures, and might suggest an interesting route towards the preparation of trimers.

EXPERIMENTAL DETAILS

The experiment starts with an ultracold gas of fermionic ^{40}K immersed in an ultracold gas of bosonic ^{23}Na , both species jointly trapped in a crossed optical dipole trap (ODT) as ellipsoidal atom clouds in their respective hyperfine ground states ($|F = 1, m_F = 1\rangle$ for ^{23}Na and $|F = 9/2, m_F = -9/2\rangle \equiv |\downarrow\rangle$ for ^{40}K). The Bose-Fermi mixture is sympathetically cooled to temperatures of $\approx 100\text{ nK}$ making use of an interspecies three-body zero crossing to minimize losses. After evaporation, the ODT has trapping frequencies $2\pi \times (108, 112, 9)$ Hz,

and the bosons condense into a BEC with a typical peak density of $n_B \approx 40\mu\text{m}^{-3}$ with the fermions deeply in the impurity regime. The condensate is weakly interacting, with an interboson scattering length of $a_{BB} = 52 a_0$ where a_0 is the Bohr radius.

To study how the existence of few-body bound states affects the many-body dressing of the impurities immersed in a degenerate bosonic bath, we perform rf injection spectroscopy by driving ^{40}K into a final state $|F = 9/2, m_F = -7/2\rangle \equiv |\uparrow\rangle$ that supports shallow bound states in the impurity-boson interatomic potential. By measuring transferred population while varying the drive frequency, we map out the spectrum of the final state's many-body Hamiltonian. We control the final state's interaction strength with the bath using a magnetic Feshbach resonance and use B -fields between 100 and 120G, for which the interspecies scattering length a varies between ~ 500 and $-1800 a_0$.

An essential feature of our experiment is that the impurity is strongly interacting with the bath already in the

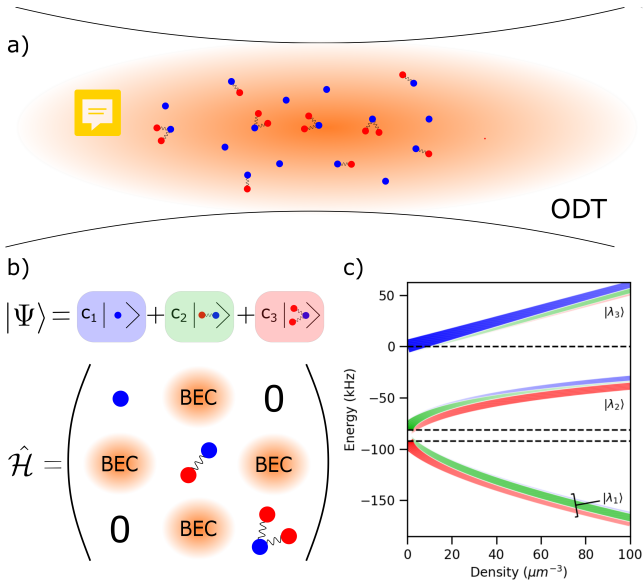


FIG. 1. Pictorial overview of our work. a) The BEC of ^{23}Na (orange), trapped in an optical dipole trap (ODT), containing ^{40}K impurities (blue) after photo-association. Some impurities bind with bosons from the BEC (in red) to form dimers and trimers. b) The wave function of a single impurity in a BEC forming a superposition of a free impurity, a dimer, and a trimer, and the effective Hamiltonian in the basis of these three states. On the diagonal are the energies of these states and the off-diagonal contributions are due to the exchange of particles with the BEC. c) The energies (in kHz) and structure of the three eigenstates $|\lambda\rangle$ of this Hamiltonian as a function of the density of the BEC in μm^{-3} . The widths and opacities of the colored sub-lines indicate the size of the coefficients (as shown in b)) $|c_1|^2$ (blue), $|c_2|^2$ (green) and $|c_3|^2$ (red) for each of the eigenstates. The horizontal dashed lines indicate the energies of the three basis states in absence of a background BEC.

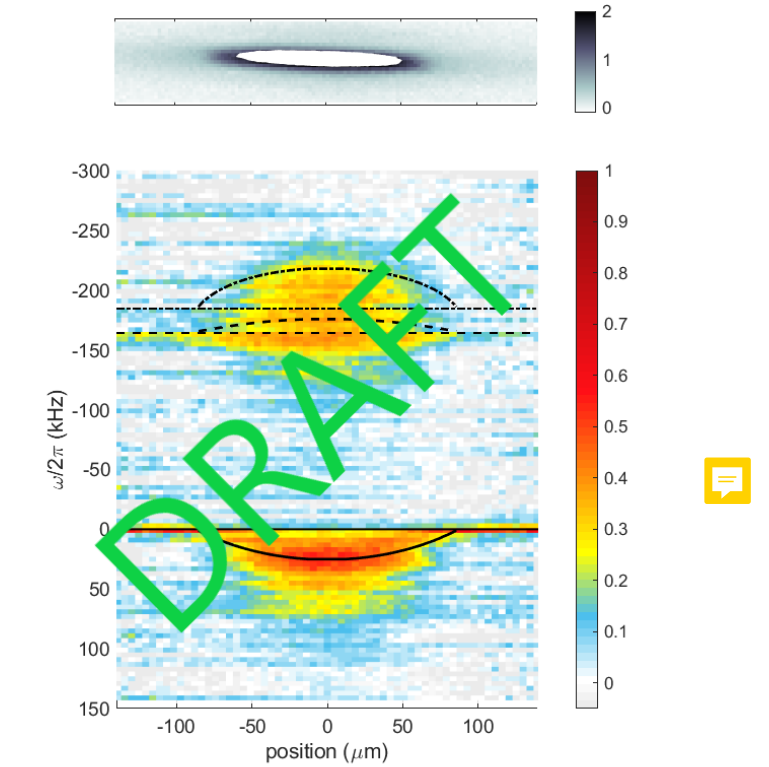


FIG. 2. [FIGURE DRAFT IN PROGRESS] The population transfer from impurity spin state $|\downarrow\rangle$ depends strongly on its position within the BEC. We show spatially resolved spectra at $B = 102.5\text{G}$ measuring the remaining population in $|\downarrow\rangle$ as a function of displacement along the long axis of the cigar shaped trap. Impurities deeply immersed in the BEC show striking deviations from theory predictions only allowing for a single excitation on top of the BEC.

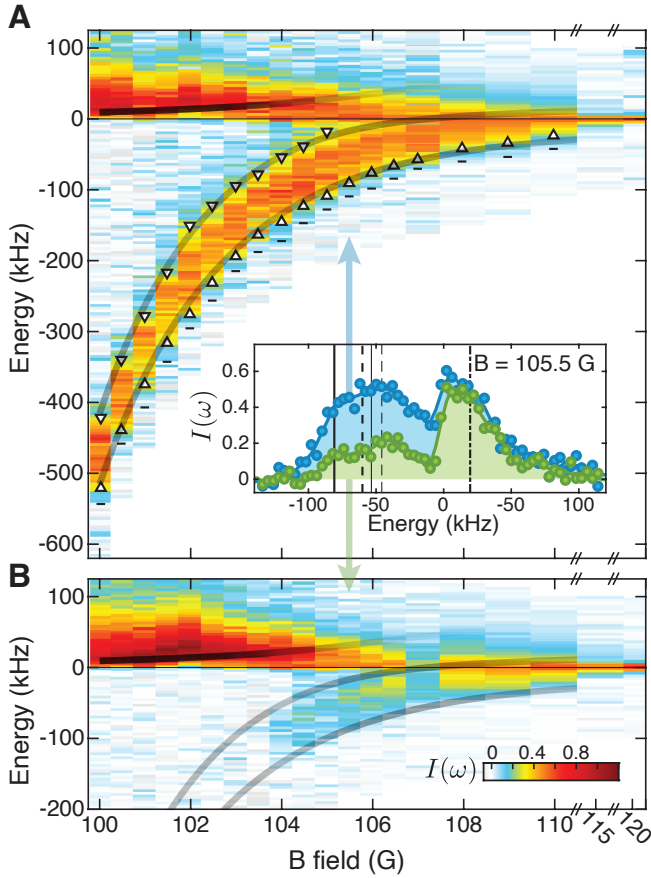


FIG. 3. Measurement of the RF transfer fraction in the center of the BEC via (A) depletion of $|\downarrow\rangle$ and (B) arrival of $|\uparrow\rangle$. Spectra are taken at various magnetic fields and plotted versus the energy of the final state with respect to the bare impurity state. In the inset a cut is shown of the obtained signal at 105.5G. In (A) the full width at half maximum of the signal is indicated by the triangles. The theory results from the three-level model are indicated via the solid lines, of which the opacity is set by the overlap of the states with the initial polaron state, weighted by the duration of the RF pulse. The horizontal black markers in (A) denote the lowest energies for which nonzero rf transfer was measured in our experiment.

initial state $|\downarrow\rangle$, with approximately constant $(k_n a)^{-1} \sim -1$, where $k_n = (6\pi n_B)^{1/3}$ is the inverse interboson distance, for $100\text{G} < B < 120\text{G}$. Indeed, we allow the impurity to form a strongly interacting attractive Bose polaron by letting it thermalize with the bath for 25ms before performing spectroscopy. This boosts the wavefunction overlap with the bound states of interest in the final many-body Hamiltonian, as the BEC density is already strongly enhanced near the impurity. This allows us to drive the rf transition to final bound states faster than their decay. As a result we are able to both deplete the initial population as well as witness the production and arrival of novel molecular states in our experiment.

To perform rf injection, we drive with frequencies

$\sim 26\text{MHz}$ using a broadband, in-vacuum antenna, providing Rabi frequency $\sim 2\pi \times 10\text{kHz}$ on the $40\text{K} |\downarrow\rangle$ to $|\uparrow\rangle$ hyperfine transition in the absence of the condensate. We drive with amplitude-modulated pulses, with the Blackman window ranging from 275 - 1600us. The pulse time is varied with the impurity-bath interaction strength, such that $\sim 50\%$ of the initial polaron $|\downarrow\rangle$ population is injected into the manifold of bound states. This is necessary as the coupling strength between the initial attractive polaron and bound states changes dramatically near the Feshbach resonance. Subsequently, populations are measured via absorption imaging. Details on the spectroscopy procedure can be found in Appendix XX.

RESULTS

A typical injection spectrum from our study can be first broadly separated into two regions, of positive and negative detuning from the bare hyperfine transition $|\downarrow\rangle$ to $|\uparrow\rangle$ in the absence of the bath. The bare transition absorbs energy from the rf drive. Therefore, transfer at negative detuning ($\omega < 0$) provides information about transitions into bound states; we call this the *attractive polaron* branch. In the few-body or equivalently low density limit, this branch corresponds primarily to the two-body bound state, i.e. Feshbach molecules of NaK. Transfer at positive detuning ($\omega > 0$) indicates an effective repulsion between the impurity and the bath particles. This leads to a local density decrease of the BEC around the impurity, and thus the formation of a *repulsive polaron*. The effective repulsion originates from the need for the eigenstates of the Hamiltonian to be orthogonal to the shallow bound state giving rise to the attractive polaron branch. Both of these branches can be seen in the spectra shown in Fig. 2.

The spatial variation in density of the bath due to the harmonic trapping potential has a strong effect on the resulting transfer $I(\omega)$. We show an example of this in Fig. 2 by spatially resolving the spectra. In the attractive polaron branch of the spectra, we make two key experimental observations that emerge as the boson density increases near the center of the BEC. First, the initial state couples into states more deeply bound than the dimer, and second, the spectroscopic feature broadens well above both the frequency resolution of the rf probe and the energy scale of the sample temperature.

Neither of these observations can be simply explained in a two-body picture. The theoretical polaron energy when limiting the calculation to at most one excitation on top of the BEC is shown as the dashed line, clearly failing to account for the main spectral feature. Instead, the role of three-body and many-body physics is crucial to understand our system in the high density regime. First, we note that in the three-body limit, an Efimov trimer state of Na + Na + K exists near the Na + K dimer state,

as is shown by the two lower dashed lines in Fig. 1C. Furthermore, the presence of a condensate strongly coupled to the impurities has two effects. The background field strongly mixes the dimer and trimer states, leading to level repulsion in the effective three-level system (solid curves of Fig. 1C) and modified decay lifetimes arising from admixture of the lossy trimer state. Finite lifetimes however are insufficient to explain the spectral widths, and thus we infer that the impurity arrives at an energy landscape that is intrinsically broad due to coupling with a dense bath.

To understand the effects of the existence of two- and three-body bound states along with the presence of a dense BEC, we use the double excitation approach as described in Ref. ..., with minor modifications. In brief, we use a single channel model with Gaussian model potentials for both the boson-impurity and boson-boson scattering. We fix the scattering length and effective range to the values found from full coupled-channels solutions of the two-body problem using realistic potentials from Refs. [1, 2]. The interboson repulsion is treated fully close to the impurity, and using the Born approximation far from the impurity. We take a variational approach as shown in Fig. 1b), allowing zero, one, or two excitations from the background condensate. We optimize the wave functions in these sectors to minimize the ground state energy of the coupled problem, and then use these wave functions to construct the simplified Hamiltonian in Fig. 1b). Thus, we have obtained our three-level model including the two excited states. None of the model parameters are fitted to the experimental results obtained in this work. Further details can be found in Appendix XX.

In Fig. 3 we see the polaron rf-spectrum as a function of the magnetic field, studying our system over a broad range of impurity-bath final interaction strengths. Focusing first on Fig. 3A, we show the spectrum obtained from measuring the atoms transferred from the initial state, and we see again the repulsive and attractive polaron branches. The black horizontal bars in Fig. 3A mark the deepest binding energies where we see spectral response, and the threshold behavior we observe on the low-energy flank of the spectra strongly suggests that we indeed observe the ground state of the final state Hamiltonian. The full width at half maximum (FWHM) of the attractive branch is indicated by the triangles, and the theory curves (opaque lines) are computed using the three-level model discussed before. The opacity of the theory curves is given by the overlap of the initial state and weighted by the rf pulse length T_{rf} , which is proportional to the transferred population for pulses within linear response. We additionally note that for $B = 115, 120$ G, the interspecies scattering length of initial and final spin states are approximately equal, so despite strong interactions, both branches collapse into a single feature given by the spectral resolution of our probe.

Our theoretical models reliably describe the FWHM frequencies of the attractive polaron branch over the wide range of interaction strengths explored. Both the lower edge of the spectrum agrees well with the ground state from the double excitation model, but also the upper edge of the spectrum agrees well with the second state in our three-level model. This indicates that an essential mechanism setting the width of the spectrum is the BEC-induced coupling between the different “bare” particle-number bound states, as shown by the off-diagonal matrix elements in Fig. 1B. Our models accounting for the many-body correlations due to the BEC are sufficient to predict the spectral location and width, but the accurate computation of the full spectral lineshapes is beyond current theoretical approaches. Our experiment provides an excellent testbed for developing theory that also includes the mechanisms of three-body loss and adding phononic excitations on top of the molecular states.

We remark that the peaks of the repulsive polaron branch of the spectra deviate from its theoretical repulsion energy, as shown by the upper opaque line in Fig. 3A. This is however unsurprising since the spectral weight depends not only the available density of states, but also the wavefunction overlap between states. The overlap of the attractive polaron with the repulsive polaron state decreases with increasing impurity-boson repulsion. The overlap in this case is stronger with the levels below the repulsive polaron state.

We can compare the depletion signal from Fig. 3A to Fig. 3B, where we show the number of arrived atoms in the final state. A quantitative analysis allows us to infer the decay lifetimes $1/\Gamma$ of the states prepared during the rf injection pulse time. We model transfer between populations P_\downarrow, P_\uparrow as $dP_\downarrow \propto -\Omega_R(t)^2 P_\downarrow dt$, where the Rabi frequency Ω_R is time-dependent due to pulse shaping, and the loss in $|\uparrow\rangle$ as $dP_\uparrow + dP_\downarrow = -\Gamma P_\uparrow dt$. We first are able to observe the arrival of the upper repulsive polaron branch, where losses are weak. However, in the attractive branch the arrival signal is much weaker. The origin of this effect is the final state being short-lived compared to the rf pulse duration. It is no surprise that the final states are short lived, since they are predicted to contain a large trimer fraction, and the trimers have a short lifetime due to three-body recombination. We find that the lifetime decreases substantially with increasing binding energy. Qualitatively this is to be expected, since the probability that the three particles meet each other at short distance and undergo the recombination reaction increases along with the binding energy.

CONCLUSION/OUTLOOK

Our study provides experimental observation of conceptually novel molecular states in a superposition of two- and three-body bound states, induced by coupling

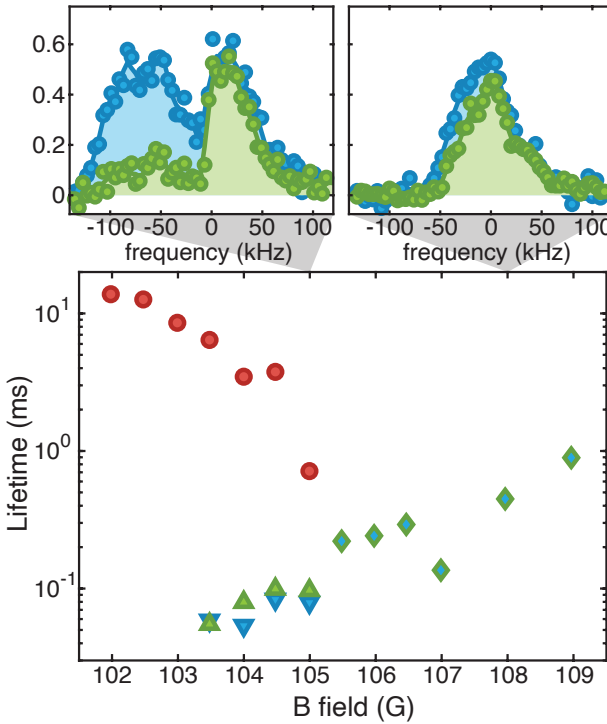


FIG. 4. The lifetimes of the states created by rf injection are inferred from the ratio of population depleted from $|\downarrow\rangle$ to population observed in $|\uparrow\rangle$, as shown in Fig. 3. Population transferred to $|\uparrow\rangle$ during the rf pulse can decay rapidly due to three-body recombination. For data taken at $B \leq 105\text{G}$, we are able to resolve the attractive and repulsive branches of the spectrum, whereas for larger magnetic fields the two features merge. This can be seen in the exemplary spectra shown in the top row. The lifetime of the bound states (triangles) decreases at deeper binding energy (away from the Feshbach resonance), whereas the lifetime of the repulsive polaron branch (circles) increases. At sufficiently deep binding energies, we do not observe any population in $|\downarrow\rangle$.

to a degenerate bosonic bath. We find that the mixing induced by the background field causes strong level repulsion, setting one of the dominant energy scales in our spectra. We show that by preparing an initial metastable polaronic state, we are able to probe the unexplored crossover between few- and many-body physics of fermions immersed in a BEC within experimentally meaningful timescales. Furthermore, our measurements provide an excellent testing ground for both existing and developing theories of polaron systems.

Our work opens the door into several new directions, spanning from fundamental questions on the role of quantum coherence in polaron physics to the present challenges in ultracold atomic and molecular gases. There are conflicting theoretical results on the finite temperature properties of the Bose polaron, and it remains to be explored to which degree the coherence that accompanies the high density and low temperature of the bosonic

bath is essential to observing the CKM-like hybridization effects. Such experiments could be implemented cleanly in homogeneous trapping potentials, where the spatial density is decoupled from temperature. We separately raise the experimental question of whether the existence and proximity of few-body bound states is a fundamentally limiting loss mechanism on the road to efficient creation and quantum degeneracy of molecular gases, when starting from degenerate atomic quantum mixtures near a Feshbach resonance [cite experimental papers]. We shed light on this process with spectroscopic precision by revealing many-body correlations and finite final state lifetimes of impurities immersed in a quantum bath.

APPENDIX: THEORETICAL MODEL

Potential calibration

To match the theoretical results to the experiment we compute the scattering length and effective range as a function of the magnetic field with coupled channels calculations using the potentials from Ref. [2]. Experimentally, we measure the dimer energy in the dilute wings of the BEC and in a separate experiment where we prepare only a dilute thermal gas. We plot the dimer energies we find, together with the theoretical prediction in Fig. . We find that the experimentally measured dimer energies agree remarkably well with the theoretical results, showcasing the high quality of the potentials from Ref. [2]. In the experimentally probed regime of magnetic fields, the dimer energy deviates from the simple formula $E_{\text{dim}} = \frac{1}{2\mu a^2}$, but agrees well if we include the effective range correction

$$E_{\text{dim}} = -\frac{1}{2\mu r_{\text{eff}}^2} \left(1 - \sqrt{1 - \frac{2r_{\text{eff}}}{a}}\right)^2 \quad (1)$$

. The root-mean-square discrepancy between the theoretical and experimental results is approximately 3 kHz, and the same for both experimental datasets. There is a region between 103 and 106 G, where the experimental data lie systematically up to kHz below the theory curve. For our polaron calculations we replace the physical interaction potential between the Na and K-atoms by a single-channel Gaussian model potential

$$V_{IB}(\mathbf{r}) = \frac{g}{2L_g^2} \exp\left(-\frac{r^2}{L_g^2}\right), \quad (2)$$

with the same scattering length and effective range. Here g sets the coupling strength and L_g the range of the potential. We do this separately for every magnetic field. The dimer energy computed using this potential has negligible deviations from the universal curve and the same

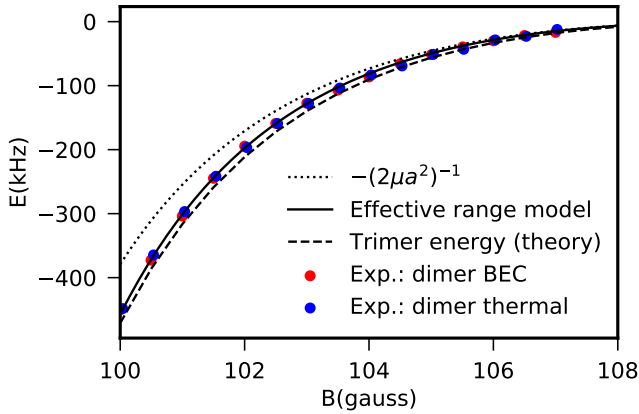


FIG. 5. Dimer energy as measured from experiment compared to the universal theoretical predictions.

holds true for the dimer energies computed from the realistic potentials from Ref. [2].

The same procedure of extracting the scattering length and effective range from the coupled channels calculation and then using them to construct Gaussian model potentials, is also used for the initial state of the spectroscopic protocol.

Similarly we compute the scattering length and effective range for the Na-Na scattering, using potentials from [1]. Over the magnetic field range of interest we find that the scattering length is approximately $56.5a_0$ with variation of only $0.2a_0$, which we neglect. In this case there does not exist a single Gaussian potential without bound states with the correct combination of scattering length and effective range. Therefore, we use a sum of two Gaussian potentials

$$V_{BB}(\mathbf{r}) = \frac{U_1}{2L_{U1}^2} \exp\left(-\frac{r^2}{L_{U1}^2}\right) + \frac{U_2}{2L_{U2}^2} \exp\left(-\frac{r^2}{L_{U2}^2}\right). \quad (3)$$

However, when L_{U1} , L_{U2} , U_1 and U_2 are all left as variational parameters, there are multiple sets of parameters having the correct combination of scattering length and effective range. We take $U_1 > 0$, $U_2 < 0$, $|U_2| \ll |U_1|$ and $2L_{U1} \leq L_{U2}$ to mimic the shape of the van der Waals potential. We find good combinations of parameters by computing the energy dependent phase shift for collision energies in the range from 1 μK to 4 mK, and comparing these to the results of the realistic potentials. The choice of parameters is not critical. If the scattering length and the effective range are correct, variations of the parameters lead to differences in the trimer energy on the order of 1 kHz, as long as the shape of the phase shift curve in this energy range is qualitatively approximated.

The resulting trimer energy is shown also in Fig. . We see that the trimer energy is slightly below the dimer energy over the whole range of magnetic fields shown. The dimer-trimer energy gap has a maximum around 101

Gauss of approximately 15 kHz and goes to zero close to the resonance. This means that for the trimer a good picture is a relatively tightly bound dimer with a loosely bound third atom. That is why the dimer-trimer coupling by the medium is strong.

In principle the accuracy of the calculations could be improved by also matching to the energy dependent phase shift for the boson-impurity potential. However, over the same energy range the main features in these phase shift curves follow from multichannel effects and indicate the proximity of other scattering resonances. These features can not be incorporated well in a single-channel picture. How much the trimer energy is affected by this remains a topic for further research. Note that some of these multichannel features are already incorporated via their effect on the scattering length and the effective range.

Variational procedure

We use the theoretical framework from Ref. [3]. In short, we consider the problem of an impurity in a BEC, with the aforementioned impurity-boson and boson-boson interaction potentials. We take the local density approximation and compute the polaron energy for a homogeneous BEC. We treat the background BEC on the mean-field level and displace the Hamiltonian using the unitary displacement operator. Then we take the Lee-Low-Pines transformation to go to the reference frame of the impurity. In this reference frame, we take the double excitation Ansatz for the wavefunction of the bosons

$$|\psi[\beta_0, \beta(\mathbf{r}), \alpha(\mathbf{r}, \mathbf{r}')]\rangle = \beta_0 + \int d^3r \beta(\mathbf{r}) \hat{b}_\mathbf{r}^\dagger + \frac{1}{\sqrt{2}} \int \int d^3r d^3r' \alpha(\mathbf{r}, \mathbf{r}') \hat{b}_{\mathbf{r}}^\dagger \hat{b}_{\mathbf{r}'}^\dagger |\mathbf{0}\rangle. \quad (4)$$

Here $\hat{b}_\mathbf{r}^\dagger$ is the bosonic creation operator, creating a boson at position \mathbf{r} . We write our variational parameters $\beta(\mathbf{r})$ and $\alpha(\mathbf{r}, \mathbf{r}')$ as sums of (products of) spherical Gaussian basis functions, taking into account the spherical symmetry of the problem to reduce the computational complexity.

Three-level model

For our three-level model, we first minimize the energy using the double excitation approach. Then we take our three levels to be (up to normalization)

$$|1\rangle = |\mathbf{0}\rangle, \quad (5)$$

$$|2\rangle = \int d^3r \beta(\mathbf{r}) \hat{b}_\mathbf{r}^\dagger |\mathbf{0}\rangle, \quad (6)$$

$$|3\rangle = \frac{1}{\sqrt{2}} \int \int d^3r d^3r' \alpha(\mathbf{r}, \mathbf{r}') \hat{b}_{\mathbf{r}}^\dagger \hat{b}_{\mathbf{r}'}^\dagger |\mathbf{0}\rangle. \quad (7)$$

The three-level Hamiltonian is found by computing the matrix elements of the Hamiltonian with respect to these three states. By construction, the ground state energy in this three-level model is the ground state energy also found from the variational minimization of the double excitation Ansatz.

The theoretical lines in Fig. 2 and 3 are computed by subtracting from the energies following from the three-level model the initial state energy and by computing the wave function overlap of these three states with the initial state. Note that these weights do not sum up to 100% since we are not describing the full Hilbert space. Nevertheless, we still find that the weights add up to 80% - 99%, depending on the magnetic field and the density. This means that our three levels together can capture well the wave function of the initial state.

In principle one can extract a whole spectrum for the Hilbert space truncated to two excitations. However, since there are general limitations to this approach we do not believe it to be more insightful than our three-level model. Indeed the double excitation Ansatz misses effects which are not so important for the ground state energy but more important for the spectrum. These include dressing of the molecular state by a long range polaron cloud or phononic excitations in both initial and final state. Furthermore, no three-body loss is included.

To compute the full spectrum which can be matched to the experiment remains an interesting open challenge. However, since the ground state energy, the width of the spectrum, and the spectral weight, are already well reproduced using the three-level model, we do believe that the three-level mixing we describe is the most essential ingredient in the description.

Treatment of the interboson repulsion

The most challenging part of the variational calculation is the treatment of the interboson repulsion. This is discussed in detail in Ref. [3]. There are two issues. The first is that we have treated the interaction in the background BEC on the level of the Born approximation, whereas in our double excitation Ansatz we explicitly take into account the interboson scattering process. Therefore, when unmodified, our variational Ansatz can also lower the energy of the BEC without the impurity. The second issue is that our parametrization of the wave function gives a good resolution close to the impurity, but the resolution decays further from the impurity. Therefore, the interboson scattering processes far from the impurity are not well described. Hence, we resolve these issues by well-motivated modifications of the interboson interaction term of the Hamiltonian. The original inter-

action term in the Hamiltonian is given by

$$\hat{\mathcal{H}}_U = \sum_{i=1,2} \int \int d^3 r' d^3 r \frac{U_i}{2L_{Ui}^2} \exp\left[-\frac{(\mathbf{r}' - \mathbf{r})^2}{L_{Ui}^2}\right] \\ + \frac{n_0}{2} (2\hat{b}_{\mathbf{r}}^\dagger \hat{b}_{\mathbf{r}} + \hat{b}_{\mathbf{r}}^\dagger \hat{b}_{\mathbf{r}}^\dagger + \hat{b}_{\mathbf{r}'}^\dagger \hat{b}_{\mathbf{r}}) \\ + \sqrt{n_0} (\hat{b}_{\mathbf{r}}^\dagger \hat{b}_{\mathbf{r}}^\dagger \hat{b}_{\mathbf{r}} + \hat{b}_{\mathbf{r}}^\dagger \hat{b}_{\mathbf{r}'}^\dagger \hat{b}_{\mathbf{r}}) + \frac{1}{2} \hat{b}_{\mathbf{r}}^\dagger \hat{b}_{\mathbf{r}}^\dagger \hat{b}_{\mathbf{r}'}^\dagger \hat{b}_{\mathbf{r}}, \quad (8)$$

whereas the modified version corresponds to

$$\hat{\mathcal{H}}_U = \sum_{i=1,2} \frac{1}{2L_{Ui}^2} \int \int d^3 r' d^3 r U_i^{(B)} \exp\left[-\frac{(\mathbf{r}' - \mathbf{r})^2}{L_{Ui}^2}\right] \\ + 2n_0 \hat{b}_{\mathbf{r}}^\dagger \hat{b}_{\mathbf{r}} + \sqrt{n_0} (\hat{b}_{\mathbf{r}}^\dagger \hat{b}_{\mathbf{r}}^\dagger \hat{b}_{\mathbf{r}} + \hat{b}_{\mathbf{r}}^\dagger \hat{b}_{\mathbf{r}'}^\dagger \hat{b}_{\mathbf{r}}) + \frac{1}{2} \hat{b}_{\mathbf{r}}^\dagger \hat{b}_{\mathbf{r}}^\dagger \hat{b}_{\mathbf{r}'}^\dagger \hat{b}_{\mathbf{r}} \\ + \frac{(U_i - U_i^{(B)})}{2} \exp\left[-\frac{(\mathbf{r}' - \mathbf{r})^2}{L_{Ui}^2} - \frac{\mathbf{r}'^2 + \mathbf{r}^2}{L_W^2}\right] \hat{b}_{\mathbf{r}}^\dagger \hat{b}_{\mathbf{r}}^\dagger \hat{b}_{\mathbf{r}'}^\dagger \hat{b}_{\mathbf{r}}. \quad (9)$$

In this expression we have replaced the quadratic terms $\hat{b}^\dagger \hat{b}^\dagger$ and $\hat{b} \hat{b}$ by $\hat{b}^\dagger \hat{b}$ to avoid renormalization of the background BEC and to retrieve the correct mean field value of the polaron energy. Second, we have replaced the interaction constants U_i by $U_i^{(B)}$ which are rescaled to give the correct scattering length on the level of the Born approximation, so without including interboson correlations. Then, we have added a three-body interaction term which accounts for the difference between the real coupling constants and the Born coupling constants at distances shorter than L_W . The magnetic-field independent constant L_W can be calibrated by comparing the result to an accurate computation of the trimer energy. We take a basis set so that we can match the accurate trimer energies up to less than 0.1 kHz across the whole magnetic field range studied here for $L_W \approx 10L_g$.

Altogether, the general philosophy of this approach is to describe accurately the interboson interactions close to the impurity, while saving computational difficulties by treating the interboson interactions on the level of the Born approximation far from the impurity.

-
- [1] S. Knoop, T. Schuster, R. Scelle, A. Trautmann, J. Appmeier, M. K. Oberthaler, E. Tiesinga, and E. Tiemann, Phys. Rev. A **83**, 042704 (2011).
 - [2] T. Hartmann, T. A. Schulze, K. K. Voges, P. Gersema, M. W. Gempe, E. Tiemann, A. Zenesini, and S. Ospelkaus, Phys. Rev. A **99**, 032711 (2019).
 - [3] A. Christianen, J. I. Cirac, and R. Schmidt, arXiv.

APPENDIX: SPECTROSCOPY AND DETECTION

To suppress the spectral sidelobes beyond the Fourier window $1/T_{rf} < 4\text{kHz}$ due to a finite rf pulse time

$T_{rf} \geq 275\text{us}$, we amplitude modulate the pulse with a Blackman window function, with parameter $\alpha = 0.16$. The Rabi frequency in the absence of the condensate as a function of time is then $\Omega_{Rabi}(t) = \Omega_{max}((1 - \alpha)/2 - \cos(2\pi t/T_{rf})/2 + \alpha \cos(4\pi t/T_{rf})/2)$ with $\alpha = 0.16$ and $\Omega_{max} \sim 2\pi \times 10 \text{ kHz}$. To measure the populations in each spin state $|\downarrow\rangle$ and $|\uparrow\rangle$ we perform on-resonant absorption imaging, using the corresponding σ_+ transitions to the 40K $P_{3/2}$, $F' = 11/2$ excited state hyperfine manifold. Each probe is also sensitive to the population in the complementary state, due to off-resonant scattering. We avoid contaminating the measurement of small populations in $|\uparrow\rangle$ (fraction $\lesssim 0.1$) by shelving $|\uparrow\rangle$ to an auxiliary ground hyperfine state during imaging, as described in Appendix XX.

For our relevant experimental parameter regime, the detuning to linewidth ratio is $\Delta/\Gamma \approx 17\text{MHz}/6\text{MHz} \approx 2.8$, which corresponds to an off-resonant scattering cross-section of $\sigma = \sigma_0/(1 + 4(\Delta/\Gamma)^2) \approx 0.03\sigma_0$, for on-resonant cross-section σ_0 .

We shelve the $|\downarrow\rangle$ population to an auxiliary ground hyperfine state $|F = 7/2, m_F = -7/2\rangle \equiv |\text{aux}\rangle$ to eliminate the contamination of the $|\uparrow\rangle$ imaging signal due to off-resonant scattering of $|\downarrow\rangle$. This is done before probing the population in $|\uparrow\rangle$, and afterwards the population in $|\text{aux}\rangle$ is returned to $|\downarrow\rangle$ for imaging. This shelving proce-

dure is designed to cleanly probe small (fraction $\lesssim 0.1$) populations in $|\uparrow\rangle$, whereas measuring the typical populations in $|\downarrow\rangle$ (fraction $\gtrsim 0.5$) is much less demanding.

The $1/e$ lifetime of the lower energy dimer-trimer dressed state is tens of us, constraining the time available for the shelving procedure. Thus, we implement shelving within 10us by using an optical Raman transition via the excited 40K $P_{1/2}$ state, with a maximum two-photon Rabi frequency $\gg 500\text{kHz}$, one-photon detuning $\approx 20\text{GHz}$. Both the pump and Stokes coupling derive from a single spatial mode near-resonant beam propagating normal to the quantization B-field, with two temporal frequencies satisfying the two-photon resonance condition between $|\uparrow\rangle$ and $|\text{aux}\rangle$.

The optical shelving pulse is configured for insensitivity to pulse timing and two-photon resonance frequency shifts. We adiabatically chirp the two-photon detuning over 2.5 MHz and amplitude modulate the two-photon Rabi frequency with a Blackman window function. This procedure maps to a rapid adiabatic passage in the approximate two-level system spanning $|\uparrow\rangle, |\text{aux}\rangle$ [cite Bergmann Perspective]. The round-trip fidelity of shelving and returning the population was measured to be 0.99 by probing the population in $|\downarrow\rangle$ after up to five round-trips, in the absence of the bath.